Atomic simulations of primary irradiation damage in U–Mo–Xe system

Wen-Hong Ouyang(欧阳文泓), Jian-Bo Liu(刘剑波)†, Wen-Sheng Lai(赖文生), Jia-Hao Li(李家好), and Bai-Xin Liu(柳百新)

The Key Laboratory of Advanced Materials (MOE), School of Materials Science and Engineering, Tsinghua University, Beijing 100084, *China*

(Received 24 June 2022; revised manuscript received 10 September 2022; accepted manuscript online 21 September 2022)

To shed a light on Xe bubble nucleation in U–Mo fuel from the view of primary irradiation damage, a reported U–Mo–Xe potential under the framework of embedded atom method has been modified within the range of short and intermediate atomic distance. The modified potential can better describe the interactions between energetic particles, and can accurately reproduce the threshold displacement energy surface calculated by the first-principles method. Then, molecular dynamics simulations of primary irradiation damage in U–Mo–Xe system have been conducted under different contents. The raise of Xe concentration brings about a remarkable promotion in residual defect quantity and generates bubbles in more over-pressured state, which suggests an acceleration of irradiation damage under the accumulation of the fission gas. Meanwhile, the addition of Mo considerably reduces the residual defect count and hinders irradiation-induced Xe diffusion especially at high contents of Xe, corroborating the importance of high Mo content in mitigation of irradiation damage and swelling behavior in U–Mo fuel. In particular, the variation of irradiation damage with respect to contents suggests a necessity of taking into account the influence of local components on defect evolution in mesoscale simulations.

Keywords: irradiation damage, metallic fuel, uranium alloy, interatomic potential

PACS: 61.80.–x, 61.82.Bg, 34.20.–b, 61.72.Qq **DOI:** 10.1088/1674-1056/ac9366

1. Introduction

In the efforts to replace highly enriched uranium (HEU) dispersion type fuel in research reactors with low enriched uranium dispersion fuel (LEU),[1] uranium alloys have been put forward as promising candidates in future fuel design, whose high value of uranium density compensates well for the density reduction caused by the replacement of HEU. Meanwhile, the introduction of alloy elements improves the stability of γ-U structure at room temperature, which has a body-centered cubic (bcc) symmetry and is obtained only beyond $\sim$ 770 °C in pure uranium. Given the low symmetry of orthorhombic α-U structure which is stable at room temperature in pure uranium, the utilization of γ-U alloys brings about remarkable enhancement in mechanical properties for production of cores of fuel elements. Among other common alloying elements like zirconium and niobium, molybdenum (Mo) has high solubility in γ-U and γ-U–Mo has shown relatively moderate swelling behavior under irradiation, with other benefits including high thermal conductivity and low thermal expansion.[2–4]

Among other challenges for further utilization in nuclear industry, irradiation swelling in U–Mo alloy poses threat on the stability of configuration dimension and mechanical properties of fuel under service environment, where the evolution of fission gas bubble (FGB) plays a critical role. Efforts have been paid to build reliable prediction of swelling behavior of U–Mo fuel,[5–7] among which a correlation between volume swelling and fission density, that is, ANL correlation,[3] has been put forward. However, in 2015 a post irradiation examination (PIE) report of U–Mo fuel pointed out some accelerated swelling behavior observed at low fission density,[8] which is not well captured by the ANL correlation. The deviation and uncertainty in prediction require further insight into the evolution mechanism and more elaborate modelling of the swelling behavior in U–Mo fuel.

At low fission density, most of fission gas have been observed to be constrained in intra-granular FGBs with size around 2 nm–4 nm.[9,10] In particular, those FGBs have been found to form bubble superlattice with face-centered cubic (fcc) symmetry in U–Mo matrix. Moderate irradiation swelling is shown in U–Mo fuel at the present stage. With fission density increasing, fission gas in form of inter-granular FGBs have been found to emerge in abundance, which have relatively larger size in micrometer and lower pressure than that of intra-granular FGBs. The abruption of inter-granular FGBs is believed to aggravate the swelling behavior and suggested to be correlated with grain refinement or recrystallization[11,12] observed in the later period of irradiation swelling. During recrystallization, a large number of small grains emerge from the original grain boundaries in U–Mo alloys, subdividing the original grains to their centers. Recrystallization extends remarkably the reach of grain boundary into the original grains, during which a large number of fission gas in intra-granular FGBs are absorbed into the grain boundary network. Consequently, the rapid diffusion and convergence of fission gas in grain boundary bring

†Corresponding author. E-mail: jbliu@mail.tsinghua.edu.cn

© 2023 Chinese Physical Society and IOP Publishing Ltd

about widespread emergence of inter-granular FGBs and aggravation of the swelling behavior. Therefore, the onset of recrystallization and its influential factors have received a lot of focus for swelling prediction of U–Mo fuel in mesoscale simulations.[13–16]

Although the underlying mechanism behind the nucleation and evolution of recrystallization in U–Mo is still a problem demanding further discussion, the emergence of recrystallization has been suggested to be highly correlated with defect evolution near the grain boundary, especially those of interstitial dislocation.[14–16] Meanwhile, in irradiated nuclear fuels, defects are generated continuously by cascade process induced by fission fragments with high kinetic energy. Due to the presence of over-pressured intra-granular FGBs as strong sinks for vacancy, there is a net population of interstitial during accumulation of irradiation damage. Thus, it can be inferred that a satisfying prediction of the recrystallization process requires appropriate descriptions of the generation of residual defects in cascade process and the evolution of intra-granular FGBs, for which reference information can be extracted from not only experiments, but also microscale simulations including molecular dynamics (MD).

By applying MD method, Hu *et al.*[17] investigated the thermodynamic properties of Xe bubbles with radius around 1 nm in U–Mo alloys, and an equation of state (EOS) in the form of a modified Van der Waals gas law has been fitted to the simulation results with high accuracy. It has also been observed that at the later period of bubble growth the pressure and Xe concentration of over-pressurized gas bubbles are maintained at a stable level. The release of excessive pressure is attributed to lattice deformation near the gas bubbles in form of the emission of interstitial dislocations. Based on the previous work, Beeler *et al*. reported an improved EOS of Xe bubble,[18] the applicability of which is extended with respect to temperature, pressure and bubble size. Moreover, it has been suggested that for more accurate description of bubble evolution a correlation should be further taken into consideration between bubble size and Xe concentration of equilibrated bubble, at which under-to over-pressured transition occurs. Different from above research focusing on bubble evolution near equilibrium, the present work has investigated Xe convergence and bubble nucleation from the view of primary irradiation damage, which involves heavily non-equilibrium behavior. Meanwhile, the implication of Xe and Mo content for generation of residual defect from irradiation damage has also been taken into discussion.

2. Method

2.1. Modification of interatomic potential

The LAMMPS[19] software package and the U–Mo–Xe potential utilized in the research of Hu *et al.*[17] and Beeler *et al.*[18] are employed in the present study. The ternary potential was proposed by Smirnova[20] within the framework of embedded-atom method (EAM)[21] with the following form:

$$E_i = \frac{1}{2}\sum\nolimits_{j\neq i}\phi_{ij}(r_{ij}) + F(\bar{\rho}_i), \tag{1}$$

where ϕ_{ij} and $F(\bar{\rho}_i)$ describe the repulsive interaction between ion cores in pairwise potential and the attraction effect on center atoms from electronic atmosphere provided by their adjacent atoms, respectively. Given the lack of description of atomic behaviors in short atomic distances, the ternary potential was usually splined to the Ziegler–Biersack–Littmark (ZBL) potential for cascade simulations in previous research.[22,23] However, Stoller *et al.*[24] pointed out that the implementation of interpolation between the potentials plays a sensible role in the results of cascade simulations, and proposed to validate the interpolation process by comparing the energetics description of local lattice distortions from the splined potential with that from the first-principles (FP) method. In the present study, modifications similar to those made by Stoller have also been implemented.

To be specific, the configuration evolution of local lattice distortion is sampled by translating an atom in a $3\times3\times3$ bcc supercell in several equidistant steps from its lattice site along the directions of $\langle100\rangle$ and $\langle110\rangle$. The corresponding energetic variance of the supercell is presented by ΔE_{t} as the following:

$$\Delta E_{\mathrm{t}} = E_{\mathrm{translated}} - E_{\mathrm{perfect}}, \tag{2}$$

where $E_{\mathrm{translated}}$ and E_{perfect} are single point energies of the configuration with lattice distortion and that with perfect symmetry, respectively. The energetic variances as benchmark are calculated by the Vienna *ab initio* simulation package (VASP)[25] within the framework of density functional theory (DFT). Projector augmented wave (PAW) pseudopotentials[26] and Perdew–Burke–Ernzerhof (PBE) exchange–correlation functional[27] are utilized. The kinetic energy cutoff is set to 400 eV and a $4\times4\times4$ grid with the Monkhorst–Pack method[28] is utilized.

The process of modification can be divided into three steps. First, in order to reduce the number of correction freedoms in modification, the original elemental electron density functions in the U–Mo–Xe potential are splined to a constant smoothly upon r_{ij} decreasing below 2.4 Å, which is shown in Fig. 1. In particular, pairwise potential functions for several element pairs are also modified to constants smoothly within intermediate distance, because their original function shows unreasonable uplift outside near-equilibrium range. Secondly, a preliminary potential is produced by overlaying a ZBL potential splined to zero within 1 Å–1.8 Å on the EAM potential modified in the first step. Deviations are also calculated between the energetic variances with respect to local lattice distortion described by the preliminary potential and that by DFT.

At last, a pairwise potential for compensation of the energetic deviation obtained in the second step is fitted to the deviation curve by the cubic interpolation method, and a final hybridized potential is generated by an overlay of the preliminary potential and the deviation correction potential.

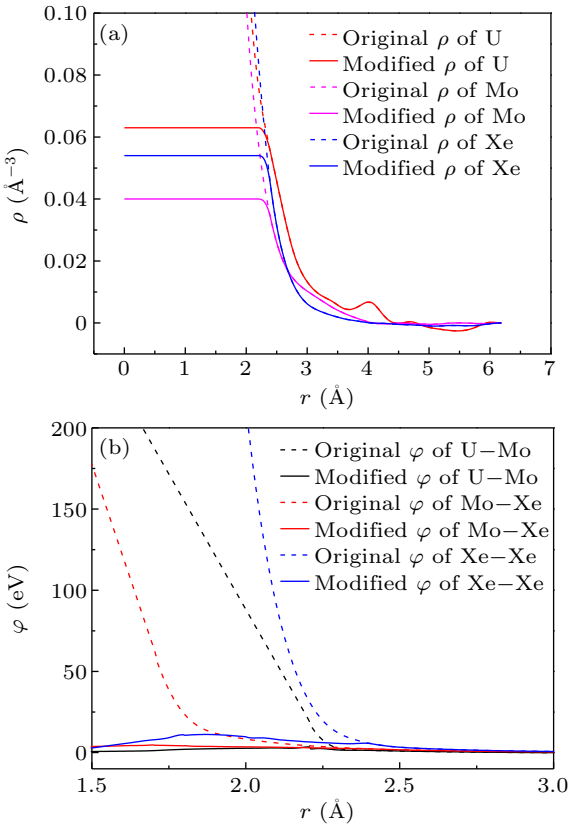


Fig. 1. The comparison between (a) original and modified electron density ρ of U, Mo, and Xe and (b) original and modified pair potential of U–Mo, Mo–Xe, and Xe–Xe.

2.2. Simulation method of cascade process

A $80 \times 80 \times 80$ supercell containing up to 1.024×10^6 atoms in bcc structure is constructed for simulations of U–Mo alloys. Contents of 7 wt.% Mo, 10 wt.% Mo, and 15 wt.% Mo have been chosen in the present study, with alloying element distributed randomly in the initial U lattices. Then, Xe atoms as substitutional impurities are introduced by replacing 0 at.%, 0.25 at.%, 0.5 at.%, 0.75 at.%, and 1 at.% of all atoms randomly, regardless of whether the original atom is a U or Mo. The simulation boxes are subsequently equilibrated in an NPH[29] ensemble at zero pressure, in which x, y and z components of the simulation box dimensions are relaxed individually with a damping parameter of 0.1. A Langevin thermostat[30] is also applied, with temperature set to 600 K. The supercells are then equilibrated under periodic boundary conditions (PBC) until their temperature and pressure reach stable levels.

To simulate cascade process, the whole atoms in the simulation box are partitioned into three layers. In the outmost layer, atoms with distance from the boundary no more than 2 Å are kept static all along the simulation to mitigate the influence of total displacement of the lattice. For the rest of atoms in the simulation box an NVE ensemble is applied, and in particular, atoms in the intermediate layer with distance from the boundary between 2 Å and 8 Å are under additional thermostat control by rescaling their velocities periodically. Thus the local temperature in the intermediate layer remains static and excessive kinetic energy emitted from the core region of cascade process can be extracted from the box. A U atom in the vicinity of the center of the equilibrated supercell is launched with kinetic energy set to 10 keV. A total of 15 launch directions are sampled evenly in the fundamental orientation zone of bcc lattice, which is shown in Fig. 2. For each launch direction, cascade processes are simulated by six times. Meanwhile, time step increments are split into four stages. In order to capture the transient atomic interactions involving energetic particles, at the initial stage of PKA simulation, a variable time step in a range of 0.001 fs to 1 fs is used, which constricts the maximum of atom displacements between consecutive time steps to no more than 0.005 Å. The first stage lasts for 3×10^4 time steps. And then the time step is increased to 0.1 fs for the next 3×10^4 time steps. Afterwards, the time step is set to 1 fs and 2 fs successively for the last two stages, which both last for 4×10^4 time steps. Overall, a total relaxation time of around 125 ps is included in each simulation.

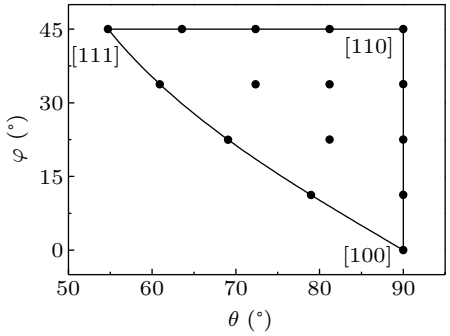


Fig. 2. A total of 15 launch directions distributed in the fundamental orientation zone of bcc lattice.

2.3. The statistical method of defect

To identify defect sites a Voronoi tessellation of atoms in the simulation box is constructed based on the initial configuration of cascade simulation, and during the simulation the Voronoi cells with occupancy equal to 0 and larger than 1 are labeled as vacancy and interstitial sites, respectively. Meanwhile, those atoms occupying interstitial sites have also been labeled and recorded as interstitial atoms. To shed a light on the interactions between Xe atoms and defect structure produced by irradiation damage, cluster analysis has been performed on the final frames of simulations. A total of three groups of sites and atoms are included in the cluster analysis with a cutoff of 4.1 Å, which consist of vacancy sites, Xe

atoms and interstitial atoms. The choice of the cluster components in the present study arises from the main focus on the influence of Xe atoms in generation of residual vacancy clusters as Xe bubble precursor, especially given that Xe has been reported to show a strong preference of binding to vacancies in U–Mo matrix.[18]

In previous reports,[17,18] Xe/vacancy ratio, or the Xe concentration, has been utilized in measurement of bubble state and defined as the ratio between the count of Xe atoms and lattice sites occupied by a bubble. In particular, the count of the occupied lattice sites is deduced by the volume of void region containing the bubble and the average atomic volume of U–Mo lattice. Due to the fact that those researches focused on near equilibrium evolution of Xe bubbles, in which the void region containing a growing bubble was constructed artificially in spherical form with little change in shape during the whole simulation, the volume occupied by the bubble could be approximated in a relatively simple manner. To be specific, the radius of the void could be calculated by the distance from the geometric center of the Xe atoms to the farthest Xe atom or the nearest U/Mo atom. However, in the present study Xe bubbles left at the end of cascade process usually show irregular shapes, suggesting further evolution toward equilibrium and bringing about difficulty in determining their volume with those reported methods. Meanwhile, from the view of Voronoi tessellation, the occupancy of lattice sites by a bubble with irregular form can be measured by the count of vacancy sites and Xe atoms included in the bubble identified by cluster analysis. In particular, a simplified schematic diagram demonstrating the typical structure of Xe bubbles is shown in Fig. 3. It has been found in most cases that the occupancy counts of lattice sites containing Xe atoms and interstitial atoms are equal to 1 and 2, respectively. The interstitial atoms are usually distributed at the peripheral of the bubbles, consisting mostly of U and Mo atoms, while Xe atoms prefer to bind to vacancies, tending to reside near the center of the bubbles. Moreover, it is assumed that during evolution toward equilibrium the annihilation between vacancy and interstitial defects within a bubble would be as complete as possible. Thus, in statistics of the present study, net vacancy counts of a bubble, which is defined as the difference between the vacancy sites and interstitial sites within the bubble, is utilized for approximation of equivalent vacancy count for the bubble near equilibrium.

Based on analysis and assumption above, in the present study the quantity of residual vacancy is denoted as that of net vacancies. And the lattice sites occupied by a bubble, also called as the bubble size in the following analysis, is defined as the sum of net vacancies and Xe atoms within the bubble. Moreover, Xe/vacancy ratio is defined as the ratio between the count of Xe atoms and the lattice sites occupied. In particular, only clusters with net vacancy count larger than 0 are included in the following analysis, excluding those which are actually rather interstitial clusters than Xe bubbles. There might be deviations between Xe/vacancy ratios calculated by the methods from the reported research[17,18] and the present study due to different approximations in calculation. However, the positive correlation between the calculated Xe/vacancy ratio and the corresponding bubble state including pressure and trend of absorbing vacancies have still been preserved. The present statistical scheme lays the foundation of the following analysis focusing on the apparent variation of residual defect generation rather than specific cluster structures.

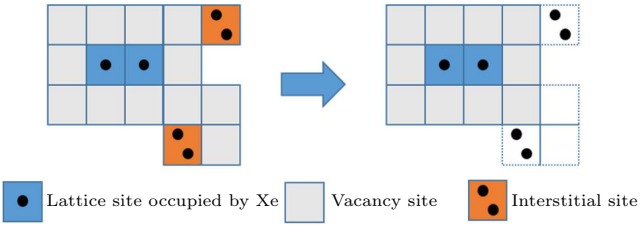


Fig. 3. The schematic diagram illustrating the equivalent bubble structure (the right matrix) near equilibrium for a bubble generated by primary irradiation damage (the left matrix). The boxes with blank background at the peripheral of the right matrix indicate vacancies and interstitials annihilated during evolution toward equilibrium.

3. Results and discussion

Figure 4 shows the energetic variances of the supercell as a function of the ratio between the distance of nearing dimers and the lattice constant of bcc-U described by DFT and the hybridized potential. It could be seen that in most cases the hybridized potential reproduces the variations in well agreement. And it is also noteworthy that in Figs. 4(k), 4(l), 4(o), and 4(p), where all the three types of atoms are included within intermediate interatomic distance, the energetic variance curves are still reproduced with high accuracy.

Figure 5(a) shows the spatial distribution of residual clusters at the end of a cascade simulation. The vacancy sites are indicated by green spheres centered at corresponding Voronoi cells. It could be seen that at the center region of the simulation box a Xe bubble has formed, with a layer of vacancy sites surrounding and separating inner Xe atoms from U–Mo matrix. Meanwhile, the bubbles with smaller size or the Xe-vacancy complexes, have been found to be distributed around the core region. It could also be seen from Fig. 5(b) that relatively longer displacements of Xe occur mainly in the core region of cascade, where those Xe atoms converged into the core bubble travel the longest distances. In general cascade process, void clusters are generated by transient high pressure introduced by PKA in evolution of displacement spike. In melting U–Mo alloys, Xe atoms have been found to show a higher diffusion rate than those of U and Mo atoms at high temperature.[22] And there is also a strong inclination of Xe atoms to reside in a bubble rather than in U–Mo matrix.[18]

Hence, it can be expected that the intense atomic mixing during cascade process plays an accelerating role in convergence of Xe atoms originally dispersed in U–Mo lattice, with the void cluster in the core region and surrounding vacancy complexes transient during cascade process as possible nucleation sites of Xe bubbles.

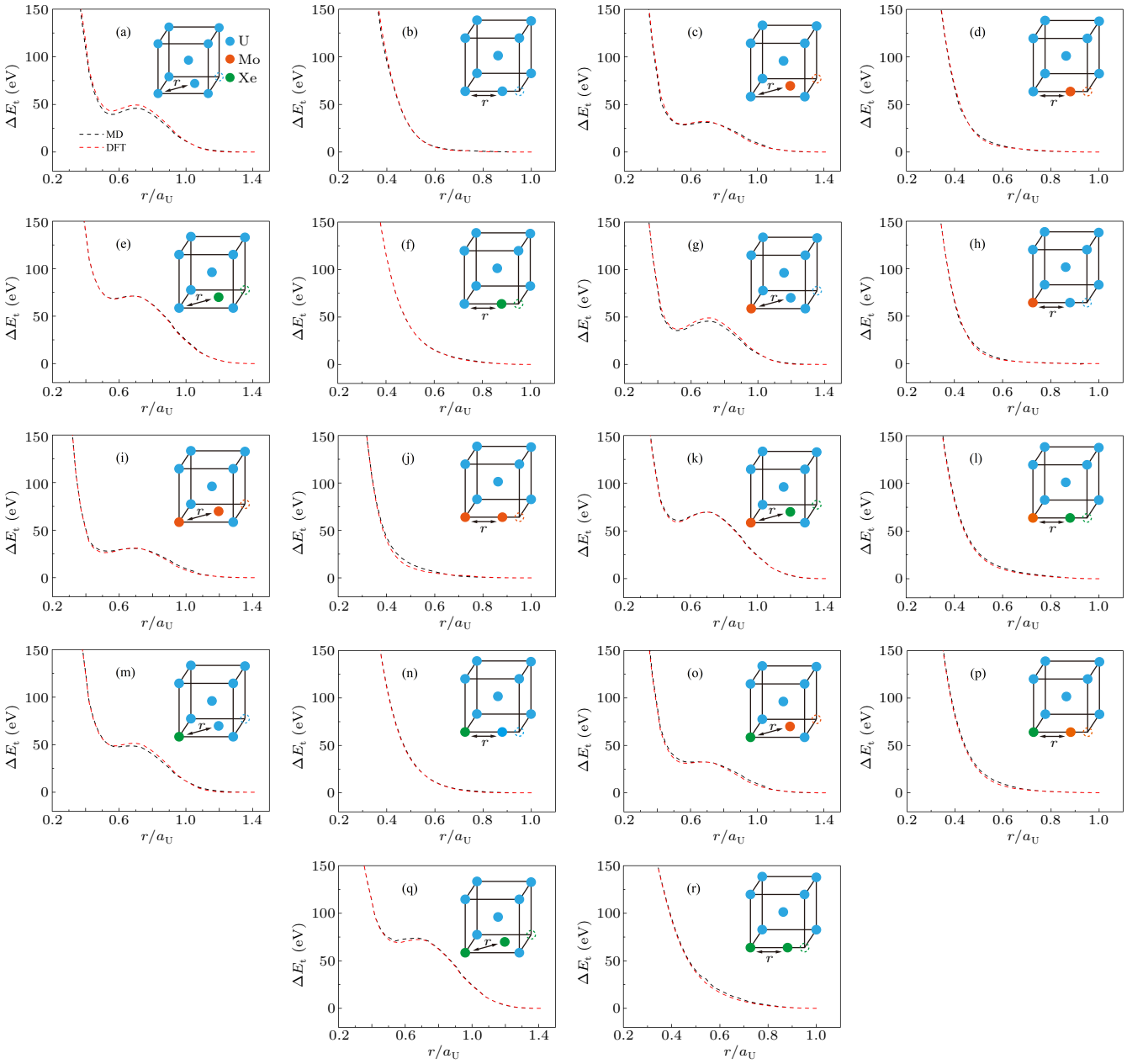


Fig. 4. The energetic variations of the supercell as a function of the ratio between the distance of nearing dimers and the lattice constant of bcc-U. Nearing diatoms include element pairs of (a) U–U in ⟨110⟩, (b) U–U in ⟨100⟩, (c) U–Mo in ⟨110⟩, (d) U–Mo in ⟨100⟩, (e) U–Xe in ⟨110⟩, (f) U–Xe in ⟨100⟩, (g) Mo–U in ⟨110⟩, (h) Mo–U in ⟨100⟩, (i) Mo–Mo in ⟨110⟩, (j) Mo–Mo in ⟨100⟩, (k) Mo–Xe in ⟨110⟩, (l) Mo–Xe in ⟨100⟩, (m) Xe–U in ⟨110⟩, (n) Xe–U in ⟨100⟩, (o) Xe–Mo in ⟨110⟩, (p) Xe–Mo in ⟨100⟩, (q) Xe–Xe in ⟨110⟩, and (r) Xe–Xe in ⟨100⟩. Calculation results from DFT and MD using the modified potential are represented by red and black dash lines, respectively. In the configuration diagrams, blue, orange and green circles represent U, Mo, and Xe atoms, respectively, and the original positions of displaced atoms are indicated by dotted circles.

To analyze quantitatively the influence of Xe in residual defect generation, Fig. 6 shows the variation of lattice and vacancy sites occupied within all residual bubbles as functions of Xe content under different Mo concentration. It can be seen that under all the Mo contents, significant promotions in lattice site and residual vacancy count have been observed with Xe content increasing, especially upon reaching the content of 0.25 at.% Xe. Correspondingly, it can be expected that much more residual interstitials are also generated at higher Xe content. The prominent positive correlation suggests an acceleration of irradiation damage under the accumulation of Xe, and can be attributed to the strong preference of Xe to capture vacancies generated during cascade process. Meanwhile, it has also been found that the addition of Mo reduces the sum of lattice sites and residual vacancies significantly, especially at high Xe content. The tendency can be explained by the vari-

ation of melting points of γ U–Mo solution, where the introduction of Mo increases the melting point.[31] In particular, the promotion trend in melting point by addition of Mo has been captured by the U–Mo–Xe potential.[22] And then one would expect less extent of localized melting produced at higher Mo content under the same level of kinetic energy transferred from PKA. The spatial constraint on cascade process increases the probability of defect annihilation and reduces the quantity of Xe involved in atomic mixing, lending support to the count reduction of lattice sites and residual vacancy with Mo content increasing. Given the fact that the accelerated swelling behavior in U–Mo fuel with relatively low Mo content has also been reported,[32] the alleviation by Mo of irradiation damage revealed by the present simulation corroborates the importance of high Mo content in mitigation of irradiation swelling in U–Mo fuel.

Moreover, Mo depletion along grain boundaries, among a wide range of composition banding, has been reported in the PIE[8] of U–Mo fuels in 2015, where some accelerated swelling behavior beyond the description of the ANL correlation has been observed. As the evolution of defect structures near grain boundary leads to recrystallization which can accelerate swelling behavior remarkably, it is necessary to take into account the influence of local components in generation rate of residual defect in mesoscale simulations for better description and prediction of irradiation swelling.

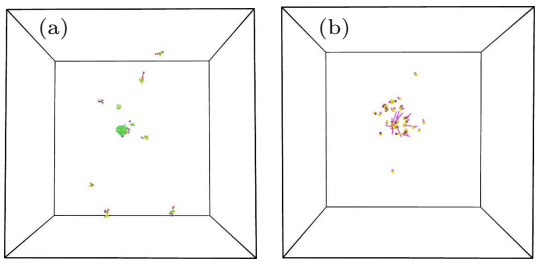


Fig. 5. A diagram of (a) spatial distribution of bubbles and (b) displacement vectors of Xe after a cascade process in U–7 wt.% Mo–0.5 at.% Xe. Only 10 clusters with largest sizes have been shown in subfigure (a), where the green, yellow, red and blue spheres represent vacancy sites, Xe atoms, Mo interstitials and U interstitials, respectively. Only displacement vectors larger than 4 Å have been shown in subfigure (b), where displacement vectors of Xe are shown by purple arrows which start from original positions and end at final positions of Xe atoms indicated by yellow spheres.

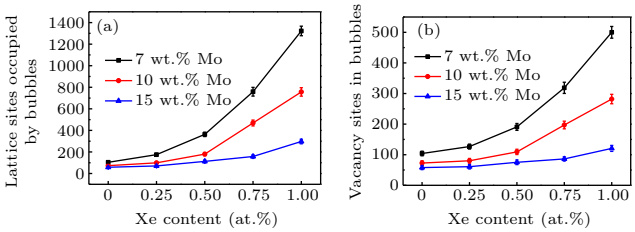


Fig. 6. The variation of (a) lattice sites and (b) vacancy sites occupied within all residual bubbles as functions of Xe content under different Mo concentrations.

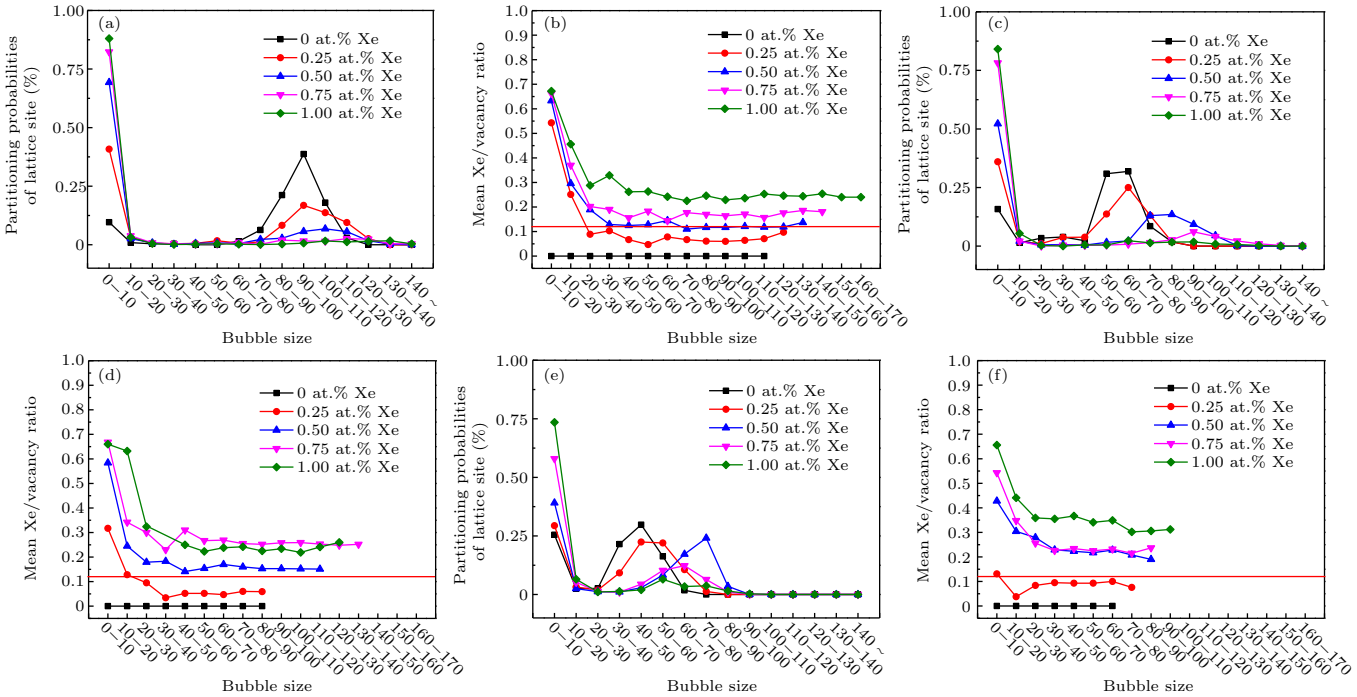


Fig. 7. The size distribution of mean lattice site partition under contents of (a) U–7 wt.% Mo, (c) U–10 wt.% Mo, (e) U–15 wt.% Mo, and mean Xe/vacancy ratio under contents of (b) U–7 wt.% Mo, (d) U–10 wt.% Mo, (f) U–15 wt.% Mo. The red horizontal line indicates Xe/vacancy ratio of 0.13. Lines between data points are only for eye guidance.

Figure 7 shows the size distribution of mean lattice site partition and mean Xe/vacancy ratio under different contents. It could be seen that with Xe content increasing there is a remarkable abruption of small bubbles with size lower than 10. In particular, the emergence of little Xe bubbles is more prominent at less Mo content, which can be explained from the view of the difference in atomic volumes. The formation of those little Xe bubbles at the peripheral of cascade region is mainly

triggered by matrix disturbance induced by central cascade process. And it can also be assumed that more alloy element with different atomic volume introduce more local lattice distortion, which can hinder long-range transfer of kinetic energy emitted from core region of cascade. Thus it can be inferred that with less Mo content, there would have higher possibility of convergence of peripheral Xe. Meanwhile, it has also been observed that the raise of Xe content brings about general promotion in Xe/vacancy ratios, indicating bubble states with higher pressure. For reference, in the previous research[18] under-to over-pressurized transition of Xe bubbles with diameter ranging from 3.1 nm to 8.5 nm has been observed to occur at Xe/vacancy ratio interval of 0.13 to 0.2, and the transition point of Xe/vacancy ratio decreases with bubble diameter decreasing. Considering that the largest bubbles generated in the present study with size around 150 correspond to bubbles with diameter around 2.2 nm near equilibrium, it can be inferred approximately that at Xe content no less than 0.5 at.%, most residual bubbles are over-pressured, with strong inclination to repel interstitials and absorb vacancies in future evolution. This finding further corroborates the aggravation role of Xe accumulation in irradiation damage.

In particular, further attention has been paid to the largest bubbles at core region with their size usually no less than 20. Figure 8 shows the mean bubble size and Xe count in core bubbles as functions of Xe content under different Mo concentrations. A general rise in bubble size and Xe quantity can be seen with Xe content increasing. However, under Mo concentration more than 7 wt.% the swelling trend of core bubbles is slowed or interrupted upon reaching high Xe contents. The aggregation behavior of Xe at high content in melting U–Mo alloys has been found to be so remarkable that the mean squared displacement (MSD) of Xe atoms decreases obviously compared to that of U and Mo atoms during simulations.[22] It can be speculated that local aggregation triggered more frequently at high Xe content during cascade process hinders Xe atoms from diffusing across longer distance and forming into larger bubbles at the end of cascade processes. Meanwhile, the earlier slowdown in bubble size at higher Mo concentration also suggests that the convergence behavior of Xe has been further impeded at high Mo content, for it promotes the melting point of U–Mo matrix and lowers diffusivity in local melting zone during cascade process. Moreover, Fig. 9(a) shows the variation of Xe MSD under different contents, which further corroborates the inhibition role of Mo in irradiation induced diffusion of Xe, especially at high values of Xe content. In particular, considering the main contribution to MSD of acute atomic mixing at the initial period of the simulation, which is shown in Fig. 9(b), the mitigation of Xe diffusion behavior at higher Mo content can also be attributed to the promotion in melting points of U–Mo matrix, which can limit the range and extent of atomic mixing during the cascade process.

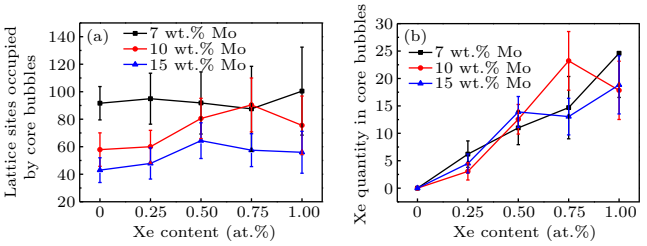


Fig. 8. The variation of (a) lattice sites and (b) Xe counts in core bubbles as functions of Xe content under different Mo concentration.

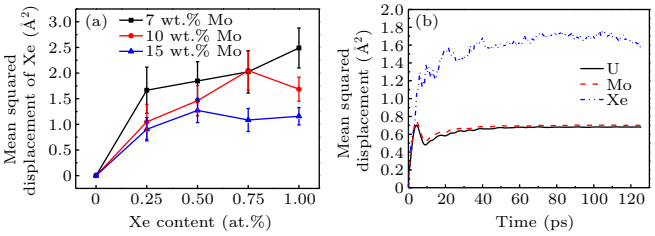


Fig. 9. (a) The variation of mean squared displacement of Xe as functions of Xe content under different Mo concentration and (b) the mean-squared displacement for U, Mo, and Xe in a cascade process in U–7 wt.% Mo–0.5 at.% Xe as a function of time.

4. Conclusion

To capture transient interatomic interaction involving energetic particles in U–Mo–Xe system, a reported ternary EAM potential has been overlaid by ZBL potential and further corrected at intermediate atomic distance, which reproduces in excellent agreement the threshold displacement energy surface calculated by DFT. In particular, the reproduction has been kept at high level of accuracy even in situations implicating all the three elements within intermediate atomic distance. The modification paves the way for more accurate simulations of irradiation damage in the U–Mo–Xe system.

MD simulations of primary irradiation damage have shown that with Xe content increasing there is a remarkable promotion of residual vacancies captured by bubbles in more over-pressured state, leaving correspondingly a large number of residual interstitials. Given the potential driving role of the evolution of interstitial dislocations in the onset of recrystallization, a positive correlation can be deduced between the accumulation of the fission gas and the aggravation of irradiation damage and swelling behavior. Meanwhile, high content of Mo has been observed to reduce the residual defect quantity significantly and hinder irradiation-induced diffusion behavior of Xe especially at high content of Xe. It lends support to the mitigation role of Mo in irradiation swelling and partially explains the detrimental potential of Mo depletion along grain boundaries observed in in-pile U–Mo fuels in terms of accelerated onset of recrystallization. Moreover, considering compositional banding observed widely in U–Mo fuel under service environment, the variation of irradiation damage with respect to contents shown by the present study could serve as

reference for more elaborate modelling of swelling behavior in mesoscale simulations.

Acknowledgments

The authors acknowledge Yi Wang for providing inspiration for dealing with technical problems. Project supported by the National Key Research and Development Program of China (Grant No. 2017YFB0702401) and the National Natural Science Foundation of China (Grant No. 51631005).

References

[1] Snelgrove J L, Hofman G L, Meyer M K, Trybus C L and Wiencek T C 1997 *Nucl. Eng. Des.* **178** 119
[2] Landa A, Söderlind P and Turchi P 2011 *J. Nucl. Mater.* **414** 132
[3] Kim Y S and Hofman G L 2011 *J. Nucl. Mater.* **419** 291
[4] Kalashnikov V V, Titova V V, Sergeev G I and Samoilov A G 1959 *Sov. At. Energy* **5** 1315
[5] Rest J, Hofman G L and Kim Y S 2009 *J. Nucl. Mater.* **385** 563
[6] Kim Y, Hofman G, Rest J, Shevlyakov G and Riar S 2008 *Technical Report No. ANL-08/11*
[7] Meyer M K, Hofman G L, Hayes S L, Clark C R, Wiencek T C, Snelgrove J L, Strain R V and Kim K H 2002 *J. Nucl. Mater.* **304** 221
[8] Williams W, Rice F, Robinson A, Meyer M and Rabin B 2015 *Technical Report INL/LTD-15-34142*
[9] Gan J, Keiser D D, Wachs D M, Robinson A B, Miller B D and Allen T R 2010 *J. Nucl. Mater.* **396** 234
[10] Van Den Berghe S, Van Renterghem W and Leenaers A 2008 *J. Nucl. Mater.* **375** 340
[11] Hofman G L, Copeland G L and Sanecki J E 1986 *Nucl. Technol.* **72** 338
[12] Berman R M 1963 *Nucl. Sci. Eng.* **16** 315
[13] Liang L, Mei Z G, Kim Y S, Ye B, Hofman G, Anitescu M and Yacout A M 2016 *Comput. Mater. Sci.* **124** 228
[14] Rest J 2004 *J. Nucl. Mater.* **326** 175
[15] Frazier W E, Hu S, Burkes D E and Beeler B W 2019 *J. Nucl. Mater.* **524** 164
[16] Hu S, Joshi V and Lavender C A 2017 *Jom* **69** 2554
[17] Hu S, Setyawan W, Joshi V V and Lavender C A 2017 *J. Nucl. Mater.* **490** 49
[18] Beeler B, Hu S, Zhang Y and Gao Y 2020 *J. Nucl. Mater.* **530** 151961
[19] Plimpton S 1995 *J. Comput. Phys.* **117** 1
[20] Smirnova D E, Kuksin A Y, Starikov S V, Stegailov V V, Insepov Z, Rest J and Yacout A M 2013 *Modell. Simul. Mater. Sci. Eng.* **21** 035011
[21] Daw M S and Baskes M I 1984 *Phys. Rev. B* **29** 6443
[22] Beeler B, Cooper M W D, Mei Z G, Schwen D and Zhang Y 2021 *J. Nucl. Mater.* **543** 152568
[23] Tian X, Xiao H, Tang R and Lu C 2014 *Nucl. Instrum. Methods Phys. Res. Sect. B* **321** 24
[24] Stoller R E, Tamm A, Beland L K, Samolyuk G D, Stocks G M, Caro A, Slipchenko L V, Osetsky Y N, Aabloo A, Klintenberg M and Wang Y 2016 *J. Chem. Theory Comput.* **12** 2871
[25] Kresse G and Furthmüller J 1996 *Comput. Mater. Sci.* **6** 15
[26] Blöchl P E 1994 *Phys. Rev. B* **50** 17953
[27] Perdew J P, Burke K and Ernzerhof M 1996 *Phys. Rev. Lett.* **77** 3865
[28] Monkhorst H J and Pack J D 1976 *Phys. Rev. B* **13** 5188
[29] Shinoda W, Shiga M and Mikami M 2004 *Phys. Rev. B* **69** 134103
[30] Schneider T and Stoll E 1978 *Phys. Rev. B* **17** 1302
[31] Rest J, Kim Y S, Hofman G L, Meyer M K and Hayes S L 2006 *Technical Report No. ANL-09/31*
[32] Van Den Berghe S and Lemoine P 2014 *Nucl. Eng. Technol.* **46** 125